In: IAC 2024 congress proceedings, 75th International Astronautical Congress (IAC), 14 - 18 Oct 2024, Milan, Italy, Paper number 86888
https://dl.iafastro.directory/event/IAC-2024/paper/86888/

# Cooperative tracking strategies for optical space-to-space surveillance constellations

**Antonio D'Anniballe[a*], Leonard Felicetti[b], Stephen Hobbs[c]**

[a] *Cranfield University, MK43 0AL, United Kingdom, antonio.danniballe@cranfield.ac.uk*
[b] *Cranfield University, MK43 0AL, United Kingdom, leonard.felicetti@cranfield.ac.uk*
[c] *Cranfield University, MK43 0AL, United Kingdom, s.e.hobbs@cranfield.ac.uk*
[*] *Corresponding author*

**Abstract**

Most space surveillance and tracking systems are constituted by networks of ground stations of observing radars and optical telescopes. These systems are usually reliable, easily serviceable, and effective under ideal conditions, but suffer from strong bounds on scalability and coverage due to the heavy constraints on their geographic locations, potential cloud coverage and the perturbing effect of the atmosphere. A large constellation of small satellites carrying optical telescopes could complement these limitations, thanks to the lack of such constraints and the possibility of observing target objects at close range. As a result, it would be theoretically possible to track objects more accurately and for longer times, improving the accuracy of collision risk analysis and manoeuvre detection amid other tasks. However, due to the small fields of view of suitable onboard optical sensors, a random static arrangement of their lines of sight would be largely inefficient in reaching good performance levels, as the target would unpredictably enter and exit the observable portion of the sky. To solve this problem, we propose a cooperative intelligent tracking strategy for the constellation. Assuming known initial states for some targets, we use predictions on the future states to dynamically control the attitudes of the constellation satellites to maximise the length of the tracking window while minimising energy expenditures. We evaluate the performance of the strategy using quality figures such as the number of effectively trackable targets and the mean square error of the estimation error during tracking. We repeat the analysis for various constellation geometries and multiple target orbits to investigate the general applicability of such a strategy. In conclusion, we check for robustness by analysing performance drops under the loss of operating nodes. The results thus obtained will inform on the usefulness of space-to-space SST constellations and the general design of strategies for the dynamic scheduling of operations of distributed systems observing multiple targets.

**Keywords:** space surveillance and tracking, orbit estimation, constellation, optical sensors

## 1. Introduction

The number of anthropogenic objects in the near-Earth space has increased dramatically in the past few years, raising the potential for collision risk [1]. To guarantee the long-term sustainability of the space environment, it is paramount to guarantee reliable conjunction alert to readily plan collision avoidance manoeuvres. To do this, timely, frequent, and accurate measurements of the state of the orbiting objects are needed for producing usable estimates. Most surveillance networks, systems aiming at achieving exactly this goal, are systems of ground sensors, mostly radars in the case of Low-Earth Orbit (LEO) objects. The main disadvantage of these systems is that they cannot be located anywhere on Earth, with the resulting strong geographic constraints harming the time availability of measurements.

In recent times, space-based optical sensors have been tested for GEO observation [2]. It has been recently proposed that networks of small satellites carrying optical sensors may be an effective way of increasing the quality of the state estimates for LEO objects [3] [4]. Although the optical requirements and potential attitude control schemes of such observer satellites have been explored, little research has been done on how to effectively set up a tracking strategy for such a network. Indeed, a lot of research exists for tasking effectively ground sensors [5], but the peculiar setup of a space-based multi-satellite system based on optical sensors remains wanting for optimal solutions.

In this paper we analyse the simplified case of a Walker-Delta constellation of observer satellites carrying optical sensors tasked with tracking a single target on a Sun-Synchronous orbit. First, we describe the setup and the chosen constellation and target parameters. We then describe the visibility and measurement model, together with their underlying assumptions. The next section describes the tracking strategy in detail, listing up all the assumptions that must be respected for the simulation to mimic a real case. Finally, we analyse the performance of the method in terms of the estimation error and tracked



Published by International Astronautical Federation (IAF). This is the Author Accepted Manuscript issued with: Creative Commons Attribution License (CC:BY 4.0).
The final published version (version of record) is available online at https://dl.iafastro.directory/event/IAC-2024/paper/86888/. Please refer to any applicable publisher terms of use.

time percentage under multiple tasking methodologies. Robustness is checked by testing multiple constellation and target geometries and by forcing measurement failures.

## 2. Scenario

We consider the case of a constellation of satellites carrying optical sensors for the observation of a single target in Low Earth Orbit (LEO). The constellation has the goal of tracking the target for as long as possible, where tracking is defined as consistent and continuous knowledge of the target state with a position accuracy of less than 1 km. In this section we characterise the constellation, the tracking, and the assumptions needed to formulate a visibility and a measurement function. The visibility function is used to understand if the target can be measured by the observer at any one time (i.e. if it is capable of reflecting light to the observing sensor), while the measurement function converts the target state into a set of measurements.

### *2.1 Constellation-Target system*

The analysed target, unless otherwise specified, is a LEO target on a circular Sun-synchronous orbit with orbital parameters $\{h, e, in, \Omega, \omega, \theta\}$ = {800 km, 0, 98°, 90°, 0°, 0°}. This parameter choice mimics an observation satellites lying near the second LEO population peak as shown in Fig. 1, making it a likely target in a real tracking scenario. The RAAN of 90° is chosen to make the orbital plane almost perpendicular to the Sun displacement vector, as we assume the simulation to take place during the Autumn equinox. This specification is important as the Sun position influences the visibility conditions as discussed in Section 2.2.

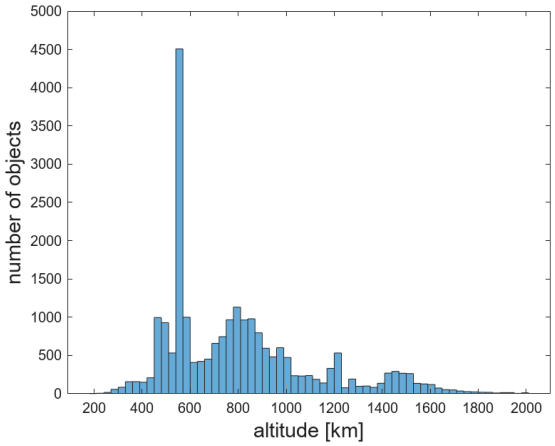


Fig. 1. Object distribution in LEO [6]

We choose a Walker-Delta constellation due to its high degree of symmetry [7]. The considered constellation is a large system comprised of $N$ = 500 observer satellites lying on circular orbits. The parameters of the constellation are summarised in Table 1. The low altitude allows for the constellation lifetime to be low enough to not cause sustainability concerns, the inclination achieves a balance between coverage of high inclinations and field-of-regard (FOR) overlapping near the poles, while a non-zero orbital phase guarantees satellites won't collide at high latitudes. The RAAN of the first orbit is left zero as it does not contribute significantly to the constellation performance for an arbitrary Sun position. The resulting constellation is shown, together with the target orbit, in Fig. 2. The visibility map of the constellation is shown in Fig. 3, where it is clear that most of the sky is covered by at least three potential measurement opportunities at any one time, while the polar region is the one offering the most measurement opportunities. To better understand why the FORs have half-disc shapes, refer to Section 2.2.

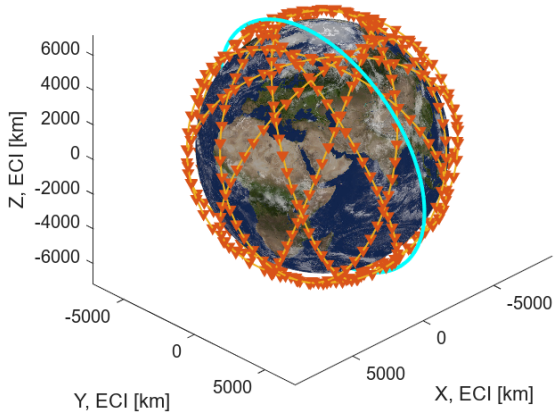


Fig. 2. Constellation and target orbit (cyan) for the constellation parameters in Table 1

Table 1. Constellation parameters

| | quantity | value | unit |
|---|---|---|---|
| $N_o$ | number of orbits | 10 | - |
| $N_{sat/o}$ | number of satellites per orbit | 50 | - |
| $h$ | altitude | 500 | km |
| $in$ | inclination | 70 | ° |
| $\Omega_0$ | right ascension (first orbit) | 0 | ° |
| $\Delta\theta$ | orbital phase | 10 | ° |

### *2.2 Visibility conditions*

A visibility condition is a condition that an observer-target pair must fulfil to allow for a measurement opportunity. We merely speak of opportunities as, for the measure-

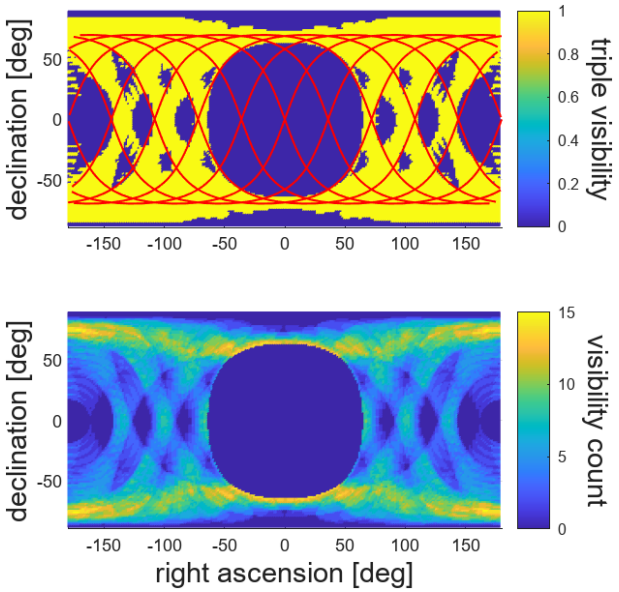


Fig. 3. Constellation visibility map ($h$ = 800 km) for the constellation parameters in Table 1. Above, the percentage of the sky where at least three observers are available. Below, the number of available observers per sky region. The hole at the centre represents the area covered by the Earth's shadow at the Autumn equinox.

ment to occur, the observer must redirect itself to point towards the target by actively changing its attitude and capturing the object within its field-of-view (FOV). The volume allowing for a measurement opportunity when a target lies in it is the field-of-regard (FOR) of the observer. The four visibility conditions are the following:

- *Shadowing, or eclipse, condition*: True if the target is outside the Earth's shadow, and therefore if it is illuminated by the Sun. This condition is independent of the observer position. Expressed as:

$$f_{e,1} := (\mathbf{r}_t \cdot \mathbf{r}_s > 0) \quad [1]$$

$$f_{e,2} := \left[ \frac{(\mathbf{r}_t \cdot \mathbf{r}_s)^2}{\|\mathbf{r}_s\|^2} - \|\mathbf{r}_t\|^2 + R^2 < 0 \right] \quad [2]$$

$$f_e := f_{e,1} \wedge f_{e,2} \quad [3]$$

- *Above-the-horizon condition*: True if the Earth is not obstructing the target view and if it is not occupying the target background. Expressed as:

$$r_{o,e} := \sqrt{\|\mathbf{r}_o\|^2 - R^2} \quad [4]$$

$$\Delta\mathbf{r} := \mathbf{r}_t - \mathbf{r}_o \quad [5]$$

$$f_o := (\|\Delta\mathbf{r}\| r_{o,e} + \Delta\mathbf{r} \cdot \mathbf{r}_o > 0) \quad [6]$$

- *Weak scattering condition*: True if the light reflected from the target reaches the observer. This is equivalent to ask that the phase angle $\alpha$ in Fig. 4 is less than 90°. For a spherical target, less than 50% of its surface is visible to the observer, enough to assume that it is too faint to be visible. It is assumed that this holds on average for the target population. It should be noted that $r_s$ is the distance of the Sun from the centre of the Earth, but since the target is much closer to the Earth compared to the Sun we can assume $\mathbf{r}_s - \mathbf{r}_t \approx \mathbf{r}_s$. The condition can be expressed as:

$$f_b := (\Delta\mathbf{r} \cdot \mathbf{r}_s < 0) \quad [7]$$

- *Limiting range condition*: True if the target is within the limiting range of the sensor of the observer. This condition arises from the fact that a target too far away will be too faint to be observable. Expressed as:

$$f_r := (\|\Delta\mathbf{r}\| - D < 0) \quad [8]$$

where $\mathbf{r}_t$ is the target position vector, $\mathbf{r}_o$ is the observer position vector, $\mathbf{r}_s$ is the Sun position vector, $R$ is the distance of the Earth's horizon from its centre (in our case, 6471 km, i.e. the average Earth's radius plus the atmospheric height), and $D$ is the limiting range. The limiting range is set to the constant value $D$ = 2000 km, a number averaging over targets of various sizes.

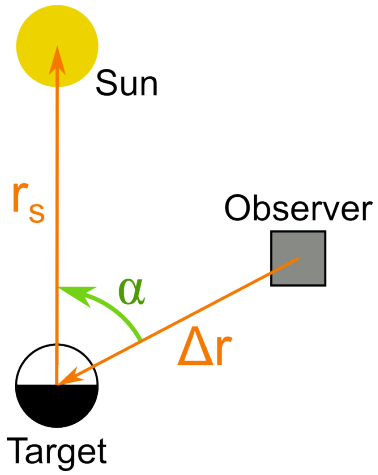


Fig. 4. Weak scattering approximation. The target is visible to the observer if $\alpha \leq 90°$.

For the purposes of this work we use a fixed value for the limiting range $D$ = 2000 km. This is only an approximation considering targets larger than 10 cm with spherical shape, assuming these represent the worst case in terms of target size and an average case in terms of light scatter-

ing. We further assume that the sensor FOVs are 5°. Some potential shapes of the resulting FOR are shown in Fig. 5.

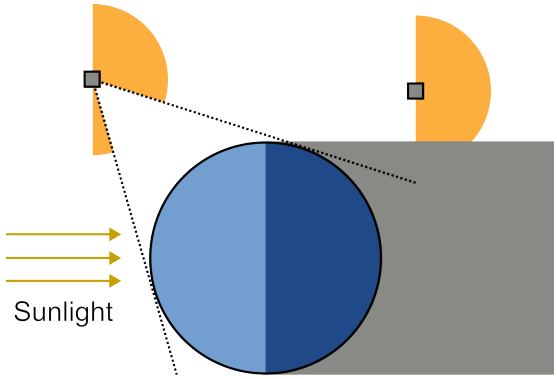


Fig. 5. Potential shapes of the field-of-regard (FOR) in orange. The observers (grey squares) can potentially observe on average any target flying in the orange region, i.e. within the FOR. Only a small portion of the FOR is actually observed due to the small sensor FOV of 5°.

### *2.3 Optical measurements*

The measurement function $\mathbf{h}(\Delta\mathbf{r}) = [\alpha(\Delta\mathbf{r}),\, \delta(\Delta\mathbf{r})]$ represents an ideal optical measurement function, i.e. a function converting the target position into its right ascension and declination component. These are the angular components of the spherical coordinates description of the target in ECI frame. This is only a simplification, as a real observer would measure the target in its local frame, and then the position in ECI would be obtained through some processing involving linear transformations. We assume this is done perfectly and therefore we incur in no information loss during the processing part. The measurement components are then simply:

$$\alpha = \text{sgn}(r_y)\arccos\frac{r_x}{\sqrt{r_x^2 + r_y^2}} \quad [9]$$

$$\delta = \arcsin\frac{r_z}{\sqrt{r_x^2 + r_y^2 + r_z^2}} \quad [10]$$

where $\Delta\mathbf{r} = [r_x,\, r_y,\, r_z]$ is the relative position of the target with respect to the observer.

Real observations are inaccurate, which means that to simulate real measurements and to properly estimate the target state we need an estimate of the sensor noise. We assume that the noise is drawn from a zero-mean normal distribution with standard deviation $\sigma_\alpha = \sigma_\delta = \sigma$, where the noises associated to the right ascension and declination are uncorrelated. The standard deviation has three components:

- *Optical noise* $\sigma_o$: Noise due to the intrinsic nature of the optical sensor. It is the maximum between the Airy disc and the pixel angular resolutions of the sensor divided by two:

$$\sigma_o = \frac{\max(\Delta_A,\, \Delta_p)}{2} \quad [11]$$

with:

$$\Delta_A = 2.44\lambda/D_A \quad [12]$$

$$\Delta_p = \sqrt{2}p/f \quad [13]$$

$\lambda$ light wavelength, $D_A$ sensor aperture, $p$ pixel size, $f$ focal length. We assume in our case $\sigma_o$ = 5 arcsec.

- *Angular uncertainty* $\sigma_\theta$: Noise due to the uncertainty on the attitude of the satellite carrying the optical payload. We assume this noise is at first order equal to the pointing error of the satellite. Assuming it is a small satellite with relatively cheap attitude determination and control system, we set $\sigma_\theta$ = 5 arcsec.

- *Position uncertainty* $\sigma_r$: Noise due to the position uncertainty of the satellite carrying the optical payload. Assuming we know the position of the satellite with an accuracy $\delta_r$ = 10 m, this is at first order:

$$\sigma_r \approx \frac{\delta_r}{r} \quad [14]$$

where $r$ is the distance of the target from the observer.

Assuming the total noise is a linear combination of its three components, the complete measurement model will then be:

$$\sigma = \sigma(r) = \sigma_o + \sigma_\theta + \frac{\delta_r}{r} \quad [15]$$

which means that the farthest the target is compared to the sensor, the higher the accuracy of the measurement. This apparently counter-intuitive result must be weighted against the fact that a farther object will appear fainter and will be more difficult to detect against the background noise. This phenomenon is captured by the limiting distance $D$, as explained in Section 2.2.

## 3. Methodology

In this section we discuss the employed methodology for target tracking, together with the underlying assumptions justifying its use in a realistic scenario. Moreover, we describe the simulation setup for testing the resulting tracking algorithm, describing as well the types of tests that we conducted and their respective goals.

### *3.1 Tracking strategy*

A tracking strategy is a way of generating a sequence of control vectors for a given set of sensors of a given time

window with the goal of maintaining state knowledge of a set of targets. In our case, the considered target is only one as described in Section 2.1. We consider only the set of tracking strategies that are:

- **Sequential**: choices of sensor tasking at each time step depend only on the information available at the current time step. The resulting strategy may be suboptimal over a finite time window as the optimisation is not carried over all possibilities over the window but the tasking choice at each step is constrained by the choice at the previous step. The advantage of such algorithms is that they can work online and are less computationally expensive, making them ideal for coordinating large networks of sensors.

- **Cooperative**: the tracking algorithm considers all sensors of the network at once. The sensor tasking is centralised, meaning that we are not optimising the tasking of each sensors but the tasking of the network as a whole. This allows for the potential disengagement of some subset of the available sensors, freeing up resources for tracking other targets.

Moreover, we assume:

- **Keplerian dynamics**: both the observer satellites and the target object follow Keplerian dynamics. Perturbations are negligible over the tracking time window.

- **Gaussian uncertainty**: the uncertainty on the state of the target can be modelled as a Gaussian noise and therefore mathematically described by a covariance matrix $\mathbf{P}$.

- **Negligible attitude dynamics**: the attitude dynamics of the observer satellites is negligible. As soon as any sensor is tasked with the observation of the target, the observer satellites points to the estimated target position instantaneously.

- **No tasking delay**: no delay is caused by tasking computation or communication to the observer satellites. Information is carried instantaneously and without failures, while computations are significantly faster than the time interval between consecutive measurements.

- **Backup surveillance and tracking system**: we assume a low-accuracy surveillance and tracking backup system is available. Such system has a fixed position accuracy of 1 km and velocity accuracy of 10 m/s. The system substitutes the constellation whenever the tracking accuracy in the form of the estimated root mean squared position error $\hat{\text{RMSE}}_r$ surpasses 10 km, for instance due to lack of measurements as a consequence of the target entering the LEO region eclipsed by the Earth. The tracking is considered lost during this time and is resumed as soon as, according to the state predicted by the backup system, some measurement is predicted to be available at the next time step. By assuming the presence of the backup system, we relieve the constellation of performing target search and object association tasks.

At each time step, the general steps of the tracking algorithm are the following:

1. **State and covariance propagation**: the state and covariance are propagated through nonlinear dynamics up to the next time step:
$$\left[\hat{\mathbf{x}}_k^-,\, \mathbf{P}_k^-\right] = f([\hat{\mathbf{x}}_{k-1},\, \mathbf{P}_{k-1}]) \qquad [16]$$

2. **Sensor tasking**: given the predicted state, a subset of the available sensors is assigned based on some criteria, ideally with the goal of maximising the information gained from the measurements at the next time step under the constraint $N_k \leq N_{max}$, where $N_k$ is the number of sensors chosen at the time step $k$ and $N_{max}$ is the maximum number of sensors to be allocated at any one time step to the tracking of the given algorithm:
$$\{s_1,\, \ldots,\, s_{N_k}\} = g(\hat{\mathbf{x}}_k^-) \qquad [17]$$

3. **Measurement collection**: given the tasked sensors, observer satellites point to the estimated target position and measurements are collected if available. In a simulation, real measurements can be obtained as:
$$\mathbf{y}_j = \mathbf{h}(\mathbf{x}_k) + \mathbf{n}(\mathbf{x}_k),\, j = 1 : \tilde{N}_k \qquad [18]$$
where $\mathbf{h}$ is the measurement function described in Section 2.3, $\mathbf{n}$ is the Gaussian noise associated to the measurements with associated covariance matrix $\mathbf{R}(\mathbf{x}_k) = \text{diag}([\sigma^2(\mathbf{x}_k),\, \sigma^2(\mathbf{x}_k)])$, where $\sigma$ is the standard deviation according to Eq. 15, and $\mathbf{x}_k$ is the real state of the target (different from the predicted and estimated ones). Notice that $\tilde{N}_k \leq N_k$ as the observer satellites point to the estimated target position and not the real one: if the estimate is off by more than the FOV of the sensor, the measurement can't be collected.

4. **Measurement update**: the target estimated state and covariance at time step $k$ are updated using the avail-

able measurements. In our case, we use an Unscented Kalman Filter (UKF) for the estimation to avoid differentiation of the dynamics and measurement functions [8]. Given the Kalman gain $\mathbf{K}$ and the measurement vector $\mathbf{y}_k$, the updates are:

$$\hat{\mathbf{x}}_k = \hat{\mathbf{x}}_k^- - \mathbf{K}[\mathbf{y}_k - \mathbf{h}(\hat{\mathbf{x}}_k^-)] \quad [19]$$

$$\mathbf{P}_k = \mathbf{P}_k^- - \mathbf{K}\mathbf{P}_{\mathbf{y}_k\mathbf{y}_k}\mathbf{K}^\mathbf{T} \quad [20]$$

If no measurements are available, the estimated state and covariance are simply set to the predicted state and covariance.

The choice of the target tracking strategy with this sequential formulation boils down to the choice of the function $g$ in Eq. 17. In all cases we first get a list of the available sensors, i.e. those sensors that could potentially be used for gaining measurements, using the visibility conditions listed in Section 2.2. We then consider three possible sensor selection methods:

- **Random**: a maximum of $N_{max}$ sensors are selected at random from the set of available ones. This is used as a control for strategy comparison.
- **Farthest**: a maximum of $N_{max}$ sensors are chosen starting from the available sensor that is the farthest from the target. This strategy is justified by the fact that the measurement standard deviation function described in Eq. 15 is inversely proportional to the target-obsever distance: the farthest the target, the more accurate the observation.
- **Random search**: the Random strategy is repeated $N_{runs}$ times to find the best set of $N_k$ observer satellites. To compute the performance of a set of satellites, we perform the measurement update step using ideal measurements and using as a metric the estimated mean squared position error of the target:

$$\hat{\text{MSE}}_r = P_{xx} + P_{yy} + P_{zz} \quad [21]$$

All sensor selection strategies are subject to two constraints:

- **Maximum amount of tasked sensors**: $N_{max} = 3, \forall\, k$, i.e. the maximum amount of used sensors at any time step is three. This is used as D'Anniballe et al. showed that this should guarantee a position estimation error within 300 m [9].
- **Repeating sensors condition**: If a sensor is available and was tasked at the previous time step, then it is tasked again at the current. This is done to avoid rapid switching between multiple satellites, which can result in the occupation of more satellites than needed and the needless expenditure of energy in the attitude control phase.

### *3.2 Simulations*

Fig. 6. Tracking using *Random* strategy and the standard constellation and target parameters listed in Section 2.1. Above, the evolution through time of the target position estimation error (blue) and of three times the RMSE (orange). Below, the number of tasked sensors (blue) and the number of tasked sensors missing their targets (orange) at each timestep.

The simulation is started for the constellation and target parameters given in Section 2.1 unless otherwise specified. Both are propagated according to Keplerian dynamics only using a Runge-Kutta solver for a time equal to the orbital period of the target. After this time, the behaviour of the tracking strategy will be approximately periodic as the period of the constellation $T(h = 500\,\text{km})/N_{sat/o}$ is much smaller compared to the target period. For the whole simulation we consider the Sun fixed at the Autumn equinox. The initial target covariance matrix is $\mathbf{P}_0 = \text{blkdiag}\left(\sigma_{r,0}^2\mathbf{I}_{3x3}, \sigma_{v,0}^2\mathbf{I}_{3x3}\right)$, where $\sigma_{r,0}$ = 1 km, $\sigma_{v,0}$ = 10 m/s. We assume we have 500 time steps, i.e. a measurement approximately every 12 s. Starting from the first time step, we repeat iteratively the tracking strategy discussed in Section 3.1 and process the resulting estimates to get useful performance metrics. The aggregate performance quantities we are interested in are:

- **Tracked time percentage**: percentage of the propagation time window for which the target is being tracked by the constellation, i.e. for which $\hat{\text{RMSE}}_r < 10$ km.

- **Median position estimation error**: median value of the position estimation error $\mathbf{r}_k - \hat{\mathbf{r}}_k$. This is favoured over other averages as it better captures the performance we expect to see for most of the time.

- **Median estimated RMSE**: estimated position RMSE, computed based on Eq. 21. This is mainly computed as a verification of the proper tuning of the Kalman filter, in which case the estimation error should be within three times the RMSE approximately 99% of the time.

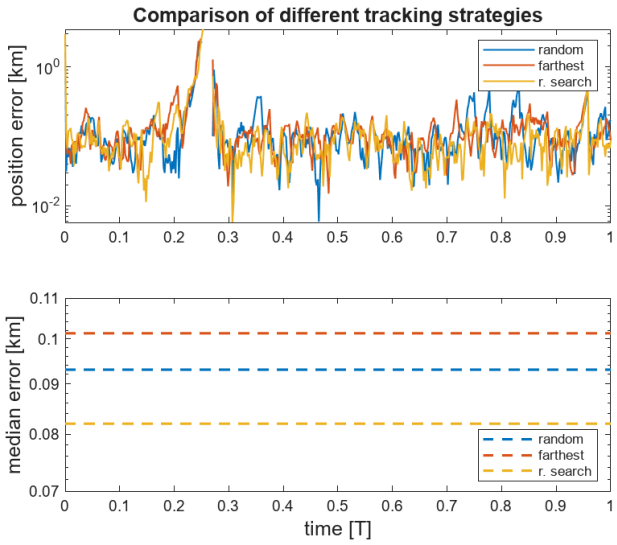


Fig. 7. Comparison of the three strategies described in Section 3.1 for the standard constellation and target parameters listed in Section 2.1. Above, the time evolution of the estimation error in the three cases. Below, the median estimation error in the three cases.

We perform four different types of analysis:

- *Strategies comparison*: we compare the behaviour of the estimation error for the three sensor tasking strategies for a single constellation and target. Moreover, we illustrate the proper tuning of the sensor by plotting the estimation error against the estimated RMSE.

- *Repeating sensors condition*: using the *Random* strategy, we illustrate the role of the repeating sensors condition in reducing sensor switching by plotting the sensor activation matrices in the cases where the condition is present and the one where it is not. A sensor activation matrix is a matrix $\mathbf{S}$ with $S_{j,k} = 1$ if sensor $j$ is activated at time step $k$, and zero otherwise.

- *Parametric analysis*: we repeat the tracking simulation for the *Random* strategy using variable constellation and target parameters to show the dependence of the tracking results on the relative geometry of the constellation-target system. Only one strategy is analysed as the tracking efficiency is much more dependent on geometry than on the tasking strategy.

- *Robustness analysis*: we repeat the tracking simulation for the standard constellation-target pair using a *Random* strategy assuming that one sensor always fails to observe the target at every time step. This is done to quantify the expected performance loss in a worst-case scenario.

## 4. Results

In this section we discuss the results of the simulations and tests described in Section 3.2.

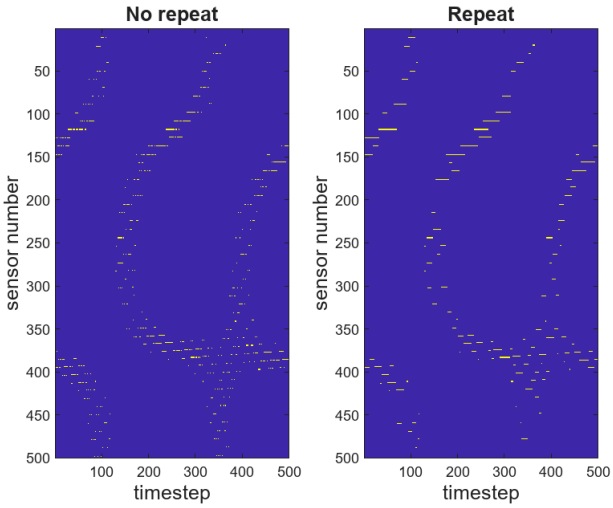


Fig. 8. Sensor activation matrices for the *Random* tracking strategies in the cases without tasked sensor repetition (left) and with repetition (right)

### *4.1 Strategies comparison*

Fig. 6 shows the time evolution of the estimation error and the RMSE for the *Random* tracking strategy case. As the estimation error is almost always within three times the estimated RMSE, this is compatible with the requirement of the estimation error being within 99% of three times the RMSE and therefore the Unscented Kalman Filter is considered to be well-tuned. We can observe that the position estimation error is in most cases within 200 m, save for the brief time the target goes in the region of space eclipsed by the Earth, when the tracking is lost for a few minutes. It is often the case that at least one sensor

misses the tasked observation, suggesting that some sky survey strategy could be necessary for increasing tracking reliability and avoiding a waste of resources. Overall, the tracking strategy seems to be effective in tracking the target accurately whenever lighting conditions allow for it.

Fig. 7 shows the comparison for the three strategies. The *Random Search* strategy, at the expense of higher computational efforts, beats *Random* by about 10% on median error. The *Farthest* strategy performs the worst among the three, possibly because it puts a strong constraint on sensor shifting. Overall, the three strategies differ only by slightly amounts in median errors, suggesting that it is more important to have a high enough number of measurements in time than to choose the best subset of observing sensors during the tasking phase.

*4.2 Repeating sensors condition*

In Fig. 8 we can observe the Sensor Activation Matrices (SAM), as defined in Section 3.2, for the cases of non-repeating and repeating sensors. When we enforce repeating sensors, observers that were tasked at the previous time step that are still available are tasked again at the current time step. The effect is clear from the image, as the non-repeating case shows many more discontinuous lines indicating a more aggressive sensor switching engaging more sensors for an higher amount of time. The SAMs also exhibit two periodic curved stroke patterns, consequence of the relative geometry of the constellation-target system. As a graphical tool, it is possible to indirectly follow the trajectory of the target through its encounters with the constellation satellites, a method which could be exploited for the efficient search of available sensors.

*4.3 Parametric analysis*

We perform three different kinds of parametric analyses to understand how the tracking strategy fares under different constellation geometries and target parameters. Fig. 9 shows the variation of performance with target altitude. We can observe that in most cases the median position estimation error remains constant at about 150 m, whereas we see a decrease in tracked time percentage, owing to the fact that farther target are reachable by a reduced number of sensors owing to the finite limiting distance $D = 2000$ km.

Fig. 10 shows the performance for variable target inclination, considering only prograde orbits. Again, the estimation error seems to be uncorrelated from the target geometry. On the contrary, targets with inclinations less than 60° exhibit much lower tracked time percentages. This can be explained by looking at the visibility map in Fig. 3, where it can be seen that targets at low inclinations always encounter the eclipsed region of the Earth, whereas

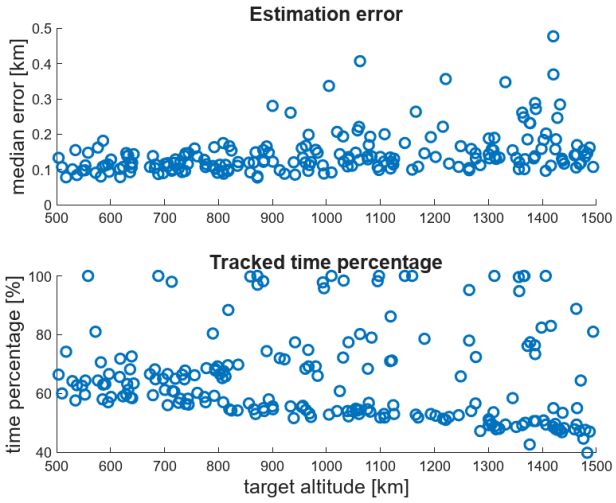


Fig. 9. Median estimation error (above) and tracked time percentage (below) for a *Random* tracking strategy, constellation parameters listed in Table 1, and target on a circular orbit with variable altitude $h$ and random inclination $in$, RAAN $\Omega$ and true anomaly $\theta$

targets at high inclinations, depending on thei RAANs, may almost completely avoid it.

Fig. 11 shows the performance behaviour for variable constellation inclination. Here, correlations are much stronger and easier to observe. For very low constellation inclinations the median estimation error suffers, as a much higher percentage of the Sun-Synchronous target orbit can't be captured by the constellation satellites. This is reflected by the linear increase in tracked time percentage, up to about 70° approximately corresponding to the higher latitude of the Earth's shadow as shown in the visibility map in Fig. 3. Further increasing the constellation inclination yields no increase in performance.

*4.4 Robustness analysis*

We analyse the case of random measurement loss, i.e. loss of one random sensor chosen at each time step among the available one, yielding always two or fewer measurements per time step. Fig. 12 shows a 30% decrease in performance, a clear worsening in median position estimation error. However, tracked time percentage is the same, and the estimation error remains most of the time below 200 m. This suggests that the strategy is robust as long as at least one measurement per time step is available, i.e. measurement frequency is invariant.

## 5. Conclusions

In this work we analysed the case of a constellation of satellites carrying optical sensors for the tracking of a Sun-

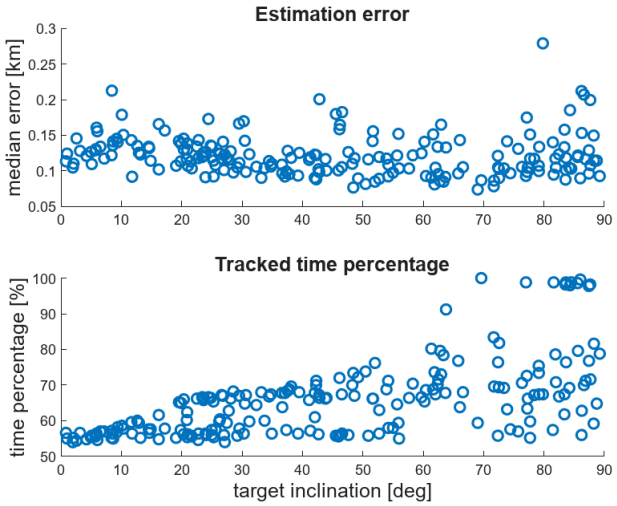


Fig. 10. Median estimation error (above) and tracked time percentage (below) for a *Random* tracking strategy, constellation parameters listed in Table 1, and target on a circular orbit with fixed altitude $h$ = 800 km, variable inclination $in$, and random RAAN $\Omega$ and true anomaly $\theta$

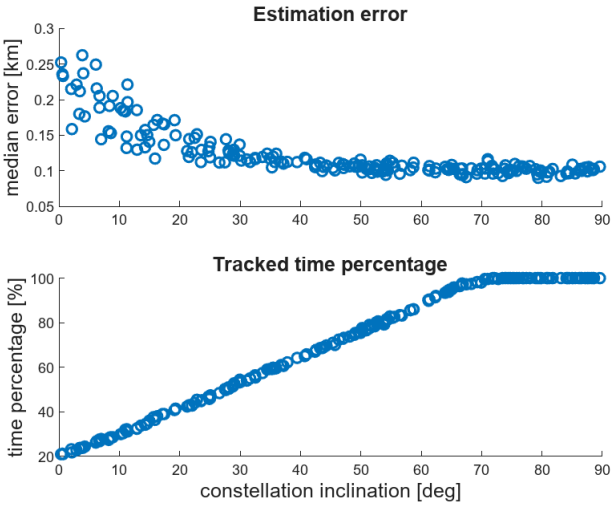


Fig. 11. Median estimation error (above) and tracked time percentage (below) for a *Random* tracking strategy, constellation with variable inclination and other parameters as listed in Table 1, and standard Sun-Synchronous target with Keplerian parameters as listed in Section 2.1

Synchronous target in LEO. We proposed a cooperative strategy for allocating in real time measurement requests to available sensors, i.e. sensors that due to the current geometry and lighting conditions are able to observe the requested target. The underlying algorithm predicts the state at the next step, computes available sensors, allocates measurements based on one of three sensor tasking strategies, and uses the resulting measurements to estimate the target state by means of an Unscented Kalman Filter.

We showed first that the strategy is capable of tracking the Sun Synchronous target with a median position estimation error of less than 150 m. We then compared the three different tasking strategies and concluded that the chosen strategy would be secondary to the capability of maintaining an high measurement frequency. By visualising the sensor activation matrix, we showed that using the constraint of reusing previously tasked sensors if available drastically reduces sensor shifting, freeing up resources that can be used for tracking other targets.

To test the robustness of the algorithm, we first tested it on multiple LEO target and constellation geometries. Estimation error resulted independent of the chosen target, while tracked time percentage decreased with target altitude and increased with target inclination. Performance correlated strongly with the constellation geometry, with tracked time percentage increasing linearly with constellation inclination up until 70° and estimation error conversely decreasing. To further test the robustness of the tracking methodology, we simulated the case of random measurement loss, showing that the amount of performance loss in that case is acceptable.

The tracking strategy was in conclusion deemed effective, reliable and robust. Research of surveillance and tracking strategies applied to networks of space-based optical sensors, however, is far from concluded. To cope with limited computational resources, we used many assumptions on the visibility conditions, and in particular we neglected target size and used strong approximations for the lighting model. More detailed analyses may test the usability of such a constellation for small debris in the 0.1-10 cm range for sustainability reason, or for large objects of irregular shapes. In a real case it is unlikely to engage the whole network for tracking only one or a handful of objects. Further research may be needed to test usable surveillance and tracking strategy for maximising the information gain over a large population of target objects.

## References

[1] ESA, *Annual Space Environment Report*, 2023. [Online]. Available: `https://www.esa.int/Space_Safety/ESA_s_Space_Environment_Report_2023`.

[2] eoPortal, *Sbss (space-based surveillance system)*, 2012. [Online]. Available: `https://www.eoportal.org/satellite-missions/sbss`.

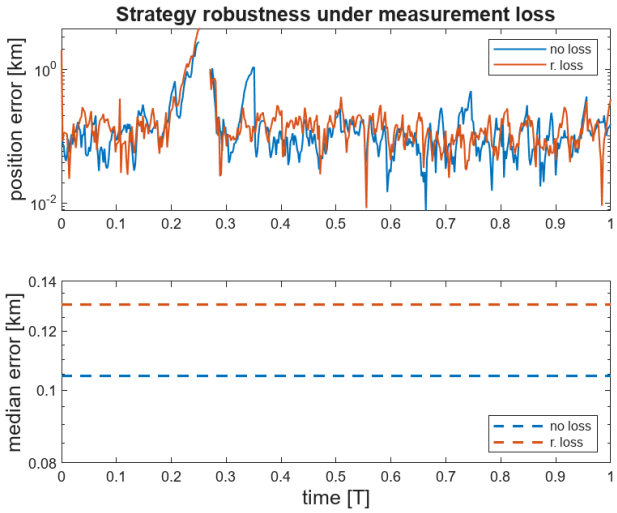


Fig. 12. Comparison of the *Random* strategy cases of no measurement loss (blue) and forced random measurement loss (orange). In the case of random loss, one random tasked sensor, chosen at each time step, always fails to observe the target. Above, the time evolution of the estimation error in the two cases. Below, the median estimation error in the two cases.


[3] L. Felicetti and M. R. Emami, "Attitude coordination of multiple spacecraft for space debris surveillance," *Advances in Space Research*, 2017. DOI: 10.1016/J.ASR.2016.12.012.

[4] D. J. Pineau and L. Felicetti, "Design of an optical system for a multi-cubesats debris surveillance mission," *Acta Astronautica*, 2023. DOI: 10.1016/j.actaastro.2023.04.027.

[5] C. Xue, H. Cai, S. Gehly, M. K. Jah, and J. Zhang, "Review of sensor tasking methods in space situational awareness," *Progress in Aerospace Sciences*, 2024. DOI: 10.1016/j.paerosci.2024.101017.

[6] *Celestrak*. [Online]. Available: https://celestrak.org/.

[7] J. R. Wertz, "Orbit & constellation design & management," in 2009, ch. 13.2.

[8] E. A. Wan and R. van der Merwe, "The unscented kalman filter for nonlinear estimation," *Proceedings of the IEEE 2000 Adaptive Systems for Signal Processing, Communications, and Control Symposium (Cat. No.00EX373)*, pp. 153–158, 2000. DOI: 10.1109/ASSPCC.2000.882463.

[9] A. D'Anniballe *et al.*, "Optimal orbital configurations of spaceborne optical sensors constellations for space surveillance," 2023. [Online]. Available: https://dl.iafastro.directory/event/IAC-2023/paper/79933/.

https://dspace.org/

# Cooperative tracking strategies for optical space-to-space surveillance constellations

**D'Anniballe, Antonio; Felicetti, Leonard; Hobbs, Stephen**

**2024-10-18**
International Astronautical Federation (IAF)
https://dl.iafastro.directory/event/IAC-2024/paper/86888/
D'Anniballe A, Felicetti L, Hobbs S. (2024) Cooperative tracking strategies for optical space-to-space surveillance constellations. In: IAC 2024 congress proceedings, 75th International Astronautical Congress (IAC), 14-18 October 2024, Milan, Italy, Paper number 86888

Downloaded from a DSpace repository. https://dspace.org/